INJURY BIOMECHANICS RESEARCH
Proceedings of the Thirty-Eighth International Workshop

Development of a Finite Element Ribcage Model of the 50th Percentile Male with Variable Rib Cortical Thickness

Z. Li, D. Subit, M.W. Kindig, R.W. Kent

ABSTRACT

In this paper, a ribcage FE model of the 50th percentile male composed of all quadrilateral and hexahedral elements were developed using an interactive multi-block hex meshing approach. The block-building and meshing techniques for reducing the model development effort and time were presented by the use of the anatomical symmetry and multiple block edition tools. Furthermore, regional variations in cortical bone thickness along the parameter and longitudinal directions of the rib structure were assigned to each of the ribs by mapping the actual cortical thickness distribution of the ribs measured in the published data. The ribcage FE model was then validated against experimental data under the hierarchical structure level from rib segment, rib ring and to full ribcage. Overall, the FE model predictions were reasonably within the range of the force-displacement corridors in experiments. This study represents a major effort in the development and validation of the thorax model for the Global Human Body Modeling Consortium. The combined hex meshing and cortical thickness mapping techniques presented here would be useful for the development of anatomically-detailed FE models to understand the biomechanics of human thorax and other human body structures.

INTRODUCTION

Thoracic injuries, primarily rib fractures, are the most common blunt trauma sustained by restrained occupants in motor vehicular crashes (Cavanaugh et al., 1993; Pattimore et al., 1992). Elderly patients (aged 65 and older) who suffer blunt chest trauma with rib fractures have a substantially higher mortality and morbidity rate than younger patients with similar injuries (Brorsson 1989; Bulger 2000; Kent 2008a; Morris et al., 2002; Stawicki et al., 2004; Stitzel et al., 2010; Wang, 2000). Although the use of advanced restraint technology and occupant protection system helps mitigate the thoracic injuries, they remain a major injury pattern in today's vehicle accidents, especially for the older population (Ridella, et al., 2007). Therefore, there is an increasing research attention to thoracic injuries of car occupants, especially for

examination of the efficacy of the restraints to the elderly, and for a better understanding of chest wall injuries resulting from a car crash (Ridella 2007).

With the improved computational capability, crash safety simulations using finite element (FE) model have been used as a powerful tool to overcome the limitations of traditional experimental methods in the study of thoracic injuries. FE models can mitigate many limitations of current test approaches that use human cadavers, human volunteers, anthropomorphic dummies and animals. Particularly, they can incorporate the complex geometry and injury prediction ability at tissue levels. However, much work remains in the development of biofidelic thorax models that adequately reflect the salient mechanics of the system. Many thorax FE models have been developed so far to investigate the structural deformation and injury responses, including isolated thorax models (Campbell et al. 2009; EI-Jawahri et al 2010; Forbes 2006; 2005; Ito et al, 2009; Kent et al 2005a; Lizée et al. 1998; Plank et al. 1998; Ruan et al., 2003; Tamura et al 2005;Vezin et al., 2009), and whole body models such as the H-model (Choi and Lee, 1999), LAB human model (Baudrit et al., 1999), RADIOSS model (Arnoux et al., 2001), THUMS model (Iwamoto et al., 2002); HUMOS model (Robin, 2001), and the Human Model from the Wayne State University (Shah et al., 2001). These existing thorax models, however, usually simplified the cortical bone geometry by use of the coarser shell elements with constant thickness, and thus were unable to reflect the regional cortical thickness variations. By use of high resolution Micro-CT data, recent studies indicated that cortical thickness substantially varies around the cross-sectional and longitudinal directions of the rib (Mohr 2007), suggesting it is crucial to model the cortical thickness variations for accurate prediction of cortical strains or injury responses of the ribs, and thus underscore the great demand for the continued development of such anatomically-detailed models. Recent advances in imaging and meshing techniques make it possible to increase the biofidelty of the ribcage model by incorporating variable cortical thickness distributions of the rib. Several researchers have incorporated the variable cortical thickness on rib segment models (Charpail et al., 2007; Li et al., 2010a and 2010b), or thorax model (Song et al. 2009; Choi 2009). Charpail et al. (2007) developed three FE models of the single 5th ribs where anatomic region-dependent cortical thickness was calculated based on segmented image contours and assigned to each of shell elements. Using bone material properties directly taken from the literature, all three FE model-predicted rib fracture locations and fracture forces well corresponded with test data. The fracture displacement and time, however, was not in good match. Li et al. (2010a) suggests that a rib model with variable cortical thickness predicts more accurate structural responses than those with constant cortical thickness. Similarly, to evaluate the thoracic deflection and injury mechanisms, Song (2009) modified the HUMOS thorax model to assign one of three discrete values of cortical thickness to the rib cortical shells in the anterior (0.4 mm), lateral (0.5 mm), or posterior region (0.6 mm) of the rib. This approach, however, still did not represent the cortical geometry of the actual rib structure as cortical thickness variation around the parameter direction of the rib cross-section was not considered. Thus, further use of high resolution micro-CT data would help accurately reconstruct regional-specific cortical thickness and improve predictions of bone fracture behaviors. Recently, Choi (2009) develop such a subject-specific thorax model for elderly Koreans with rib cortical thickness averaged from the micro-CT data of Korean males. Therefore, there is great need to develop such ribcage model that includes cortical thickness variations of the rib structures for more accurate injury prediction. To best of our knowledge, no such modeling approach to map the existing variable cortical thickness database of the rib structure was reported in the development of biofidelic ribcage model.

The objective of this study was to develop a ribcage FE model with variable cortical thickness of the rib for accurate prediction of cortical bone strains and fracture patterns. A multi-block hex meshing scheme was used to generate the high quality hexahedral meshes for the thorax model components. A novel method was developed to map the cortical thickness distribution of the ribs in the literature to individual nodes of the cortical shell elements created in this study based on the existing mesh blocks. The thickness variations in the shell elements therefore, accounted for cortical thickness variations along the perimeter and longitudinal directions of the rib structure. The ribcage model was then validated in hierarchical-structure level against experimental data from rib segment, rib ring, and ribcage.

METHODS

Finite element model development

Geometrical surfaces were obtained from a multi-modality image data collection procedure

described in Gayzik et al (2009). Volumetric hexahedral meshes of the components in the ribcage model were generated from the geometrical surface meshes using IA-FEMesh software (Grosland et al., 2009), based on multi-block hexing meshing scheme. The geometric symmetry of the human thorax was used during the block building for high quality hexahedral elements to save time in mesh generation. The final mesh density of the ribcage model was determined based on the previous sensitivity study (Li et al., 2010b). The cortical shell elements were then created for modeling the cortical bone based on the surface of the volumetric mesh. The costal cartilage was separated based on the boundary of the original medical images. The inter-vertebral disc gap was manually created by morphing the volumetric mesh to match the geometry of the vertebrae; next the solid elements that filled the inter-vertebral disc were removed and only the outer shell elements around the perimeter of the disc to connect the adjacent thoracic vertebral segments were kept. A 3-mm layer of quad-dominant shell elements were added as the inter-costal muscles to connect the adjacent ribs. The connection between the adjacent inter-thoracic vertebrae was modeled by the kinematic spherical joint. The same joint definition was used for the costal-vertebral joints to connect each rib with the thoracic vertebrae with local coordinate systems defined for three rotation degree of freedom. The resulting ribcage model (Figure 1) consisting of 83,402 solid hexahedral elements and 68,548 quadrilateral and 823 triangular shell elements.

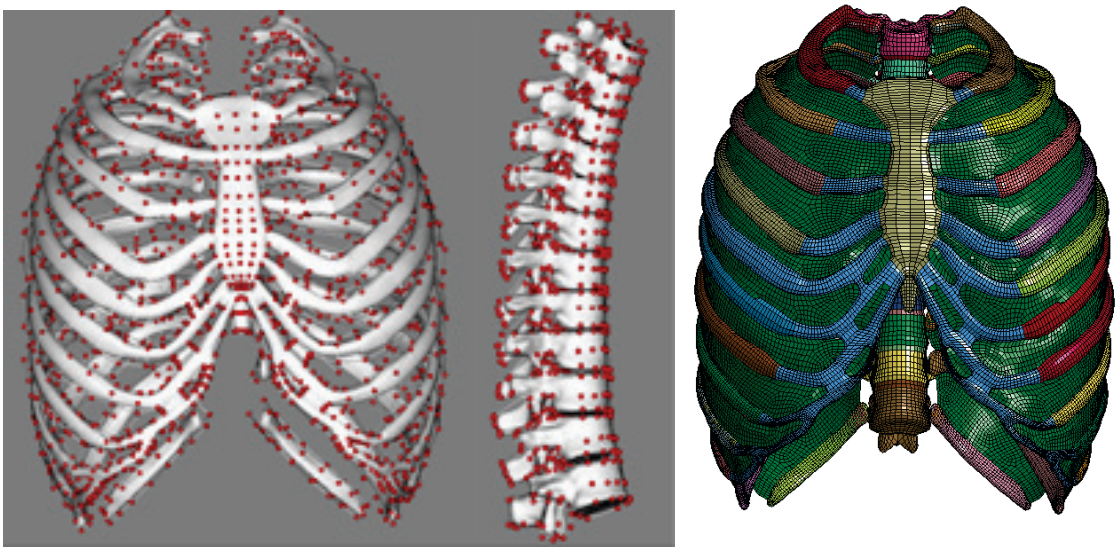

Figure 1 - An interactive multi-block hex meshing approach used to create ribcage model (left), and FE model of the ribcage with added intercostal muscles (right).

Mapping of Rib Variable Cortical Thickness

A novel mapping approach was developed using MATLAB™ to assign a unique, variable cortical thickness value to each node within the rib cortical shell meshes (Figure 2). First, the blocks used in the multi-block meshing process were discretized at 1 mm intervals along their longitudinal axes to define an approximate centroidal axis for the underlying rib. A virtual cylinder was then swept along this longitudinal axis at discrete locations, and the nodes within the cylinder bounds at each location were projected onto the plane orthogonal to the longitudinal axis to define a mesh cross-section. The centroids of subsequent cross-sections were used to define a new centroidal axis representation; this process was then repeated to provide a smoother and more accurate rib centroidal axis. Each cortical node was then assigned two normalized coordinates: its position s along the centroidal axis, and its position t around its cross-section (defined with respect to the minor principal axis of the cross-section). Each node was then assigned a cortical thickness value based on its (s,t) pair, using the Micro-CT cortical thickness data from the literature (Choi 2009).

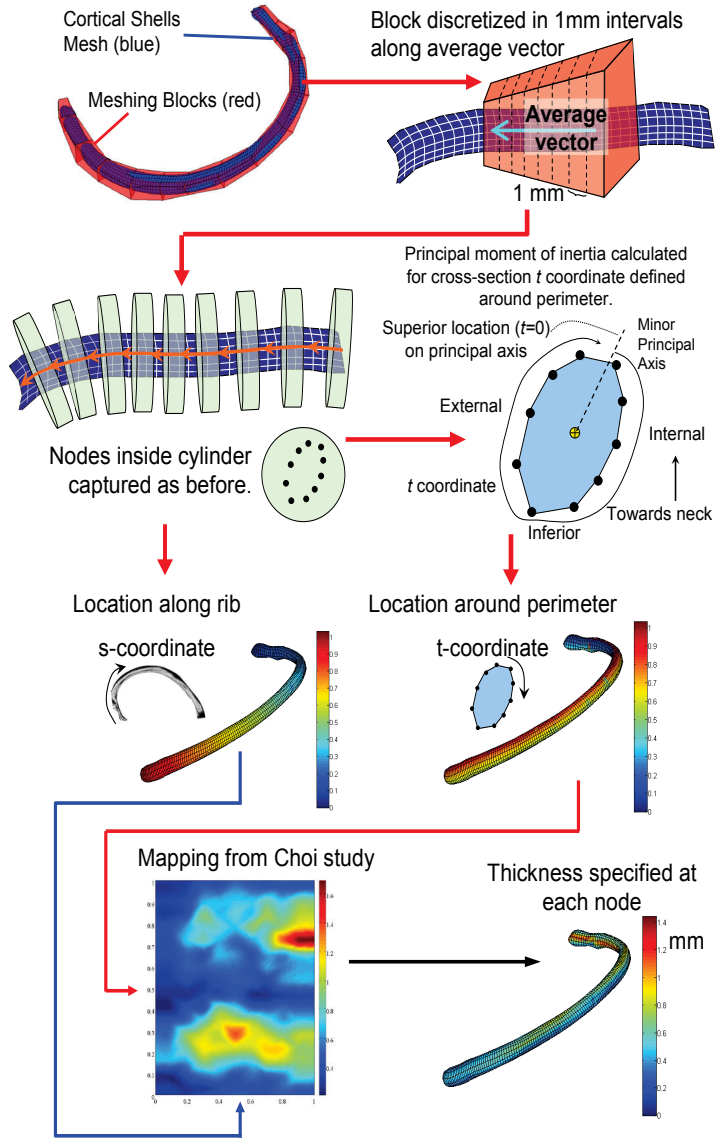

Figure 2 - Mapping nodal thickness measured from Micro-CT data to nodes of rib cortical shells.

Material properties

Cortical and trabecular bone behaviors were simulated using an elastic-plastic material model with strain-rate effect option (*MAT_03) in LS-DYNA material library. Rib fracture was defined by setting a failure plastic strain in both cortical and trabecular components, and initiated by element deletion when the plastic strain of an element reached the limit. The strain rate effect for scaling the cortical and trabecular bone yield stresses was simulated by adding the Cowper-Symonds model input using constants referred from the literature (Haug, 1994). The material properties for the rib cortical and trabecular bone were directly taken from the literature (Li et al. 2010; Zhao and Narwani, 2005). The twelve thoracic vertebral spine segments were modeled as rigid material (*MAT_20) with 0.354 GPa Young's moduli, and a Poisson's ratio of 0.3 referenced from the literature (Zhao and Narwani, 2005). The costo-vertebral joint stiffness curves were taken from the values measured by Duprey *et al.* (2010). Similarly, the thoracic spine segments were connected by spherical joints with joint stiffness curves derived from the data in Panjabi's study (1976). The costal-cartilage properties were referenced from Forman's (2010) study with a Young's modulus of 50 MPa. The cortical and trabecular bone properties of the sternum, intercostal muscles and diaphragm are referenced from the literature (Zhao and Narwani, 2005).

Model validation

Rib segment model validation under anterior-posterior loading. The first validation case regarded the rib segment that was validated against experimental data obtained for anterior-posterior bending tests (Fig. 3). A custom experimental methodology was developed to test whole ribs under in-plane anterior-posterior bending (Kindig, 2009; Li et al, 2010a). This experimental protocol has been modified from the approach published by Charpail *et al.* (2005). A total of 94 rib specimens from nine subjects were extracted from levels 2 through 10, based on specimen availability. Each rib was individually removed from the intact thoracic cage and all cartilage and other soft tissue was removed, leaving only the bony portion of the rib (cortical and trabecular components). Each rib extremity was then embedded in a two-part polyurethane compound (R1 FastCast™ 891, GoldenWest Manufacturing, Cedar Ridge, Calif.) in the major plane of the rib to provide an interface with the loading fixture (Figure 3).

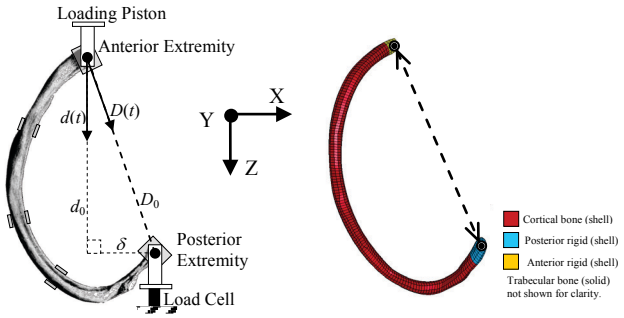

Figure 3 - Rib testing setup configuration (left). Displacement was applied in the $d(t)$ direction (left, and rib segment FE model (right).

In the experimental configuration (Figure 3, left), the anterior bracket assembly was attached to the piston of a servohydraulic testing machine, displacing the anterior extremity in the direction d while the posterior extremity remained fixed. The anterior extremity was initially positioned at an offset distance δ relative to the posterior extremity. This offset distance was defined based on the *in situ* lateral distance between the anterior and posterior extremities, measured from CT images of the whole thorax. Displacement was applied at an approximately constant velocity either quasi-statically (on the order of 2 mm/sec) or dynamically (on the order of 1 m/s) to a failure level of displacement. Reaction force and moments were measured at the base of the posterior extremity bracket, and strains were recorded. The resultant reaction force $F(t)$ and change in relative distance $D(t)$ between the anterior and posterior extremities ("end-to-end displacement") were calculated for each test and was plotted against the displacement $D(t)$ up to the time of fracture to define the force-displacement response of the rib. Each rib segment model for the 12 rib levels was created based on the anterior-posterior loading and boundary conditions (Figure 3, right). Two rotation pin joints were enforced by defining the potting portion of anterior and posterior extremities as rigid bodies with free rotation in the x-z plane and restrained translations in the y-direction. The loading was applied to the anterior extremity with the same prescribed motion and rates as those in the experiments, and the posterior extremity was the fully constrained in translation. The resultant forces versus displacement curves at rib level 2 -10 were compared to the experimental corridors for model validation.

Rib ring model validation under quasi-static loadings

The next stage in the model validation was the rib ring tests. Preliminary tests using a hub impactor on the entire thorax indicated a greater amount of rib rotation about the costo-vertebral joints than was expected: the simulations suggested that the entire rib cage simply "folded down" when loaded without fracturing, which may be a physically unrealistic scenario. This suggested that the costo-vertebral joint definitions input into the model may be too compliant to be realistic. This could be due to differences in the level of soft tissue between the Duprey *et al.* (2010) study that provided the input curves for the joints in the

FE model. The kinematic joints that defined the connection between the ribs and the vertebrae in the model were intended to encapsulate a variety of soft tissues and musculature, including the erector spinae, spinalis, rotatores, and levatores costorum that were not included in the tested specimens in the Duprey's study. These additional muscle groups may effectively make the costo-vertebral joint stiffer than the values measured by Duprey *et al.* (2010). As a result, the costo-vertebral joints warranted additional validation steps, which could be accomplished by comparing the model to the rib ring experiments. The experimental procedures of rib ring tests were summarized below (Figure 4). To prepare each rib ring, the intercostals muscles between the given rib ring and the adjacent ribs were first cut. The sternum was then cut medio-laterally along transverse lines located halfway between the costal cartilage attachment points of the present rib ring and those of the superior and inferior adjacent rib levels. This permitted the ring to move independently of the rest of the ribcage. To prevent inferior rotation of the rib ring (i.e. "sagging") during positioning or loading, the sternal section was supported by the bottom (superior-inferior) plate of an aluminum L-shaped loader. The vertebrae were fixed in place to prevent rotation or translation. The details of these experiments are described in Kindig et al.(2010).

The rib ring FE models (Figure 4, right) include the cortical and trabecular components of the two ribs at a given rib level, the associated lengths of costal cartilage, the solid rigid bodies on the posterior extremities that are used for the spherical costo-verteral joint definition, the vertebra to which these rigid bodies are attached, and a section of sternum containing the rib ring. Three parameters were considered variable for adjustment during the validation process: the costovertebral joint stiffness, the costal cartilage elastic modulus, and the sternum cortical elastic modulus. For each of these parameters, the values currently used in the model were taken as references. Six simulations were run using the model for rib ring 3. In each of the simulations, one the above parameters was increased or decreased by a factor of 100, while the other parameters were held constant. The resultant force at the end of the simulations (time 110 ms, loader displacement of 22 mm) was then compared to the model with baseline material properties

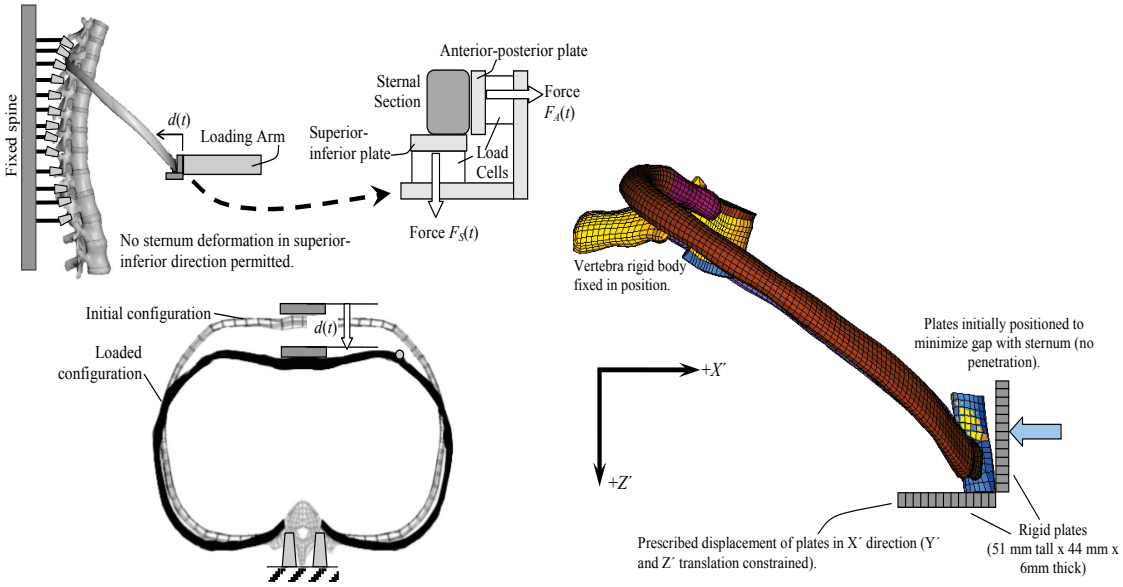

Figure 4 - Rib ring experimental setup (left) and FE model (right).

RESULTS

Variable cortical thickness of rib mapped from Micro-CT image data

Table 1 shows the range of cortical thickness, and its mean and standard deviation for each 12 rib levels that were mapped to the ribcage model, indicating large variation of cortical thickness around the edgewise and lengthwise directions within the individual rib. The mean plus standard deviation of cortical thickness in the whole ribcage was 0.67±0.37 mm. The cortical thickness contours of the whole ribcage ranges from 0.21 to 2.63 mm, and large variations were observed between different rib levels (Figure 5). For

each rib level, the anterior and posterior regions of the rib have thinnest and largest cortical bone thickness, respectively. In addition, the first rib demonstrates an overall highest mean cortical thickness compared to other rib levels.

Table 1 - Range, mean and standard deviation of the cortical shell thickness for each of 12 ribs. The weighted values were obtained by accounting for the surface area of the finite element that composed the cortical shell.

Mapped Rib Cortical Shell Thickness (mm)					
	Unweighted		**Weighted**		**Range**
Rib No	Mean	Std. Dev.	Mean	Std. Dev.	Min-Max
1	0.9210	0.4648	0.9258	0.5959	0.273-2.626
2	0.6723	0.2330	0.6321	0.2384	0.325-1.484
3	0.5409	0.1525	0.5338	0.2006	0.272-0.964
4	0.5498	0.1764	0.5509	0.2253	0.251-1.103
5	0.5853	0.2072	0.6206	0.3996	0.243-1.241
6	0.6252	0.2356	0.6301	0.2959	0.235-1.295
7	0.6252	0.2237	0.6319	0.2851	0.256-1.258
8	0.6454	0.2743	0.6791	0.4235	0.208-1.469
9	0.6976	0.3081	0.7469	0.5171	0.250-1.706
10	0.7097	0.2864	0.7611	0.4873	0.221-1.698
11	0.6403	0.2794	0.6810	0.4491	0.209-1.484
12	0.6245	0.2093	0.6576	0.3677	0.271-1.298

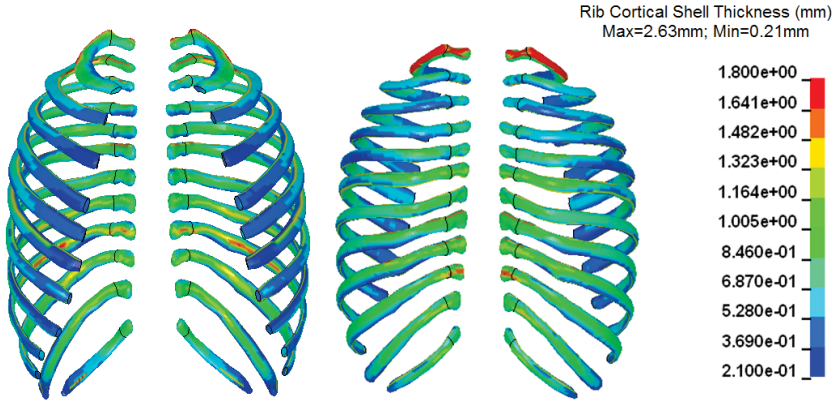

Figure 5 - Cortical thickness distribution of the ribcage mapped from the Micro-CT data.

Validation results

Rib segment model validation results. The final dataset for corridor development consisted of all specimens from male subjects, independent of loading rate and subject age. As only ribs 2-10 were tested in the experiments, corridors were only made for those rib levels. Target reaction force *vs.* displacement response corridors were then developed for each rib level using the technique described by Lessley *et al.* (2004). This technique defines the "characteristic average" as the mean response, and the corridor bounds as extending ±1 standard deviation (in both force and displacement) around the characteristic average. Note that only the response data up to the time of peak force were considered in the corridor development. Figure 6 compares these experimental corridors (gray shading) with the FE data (black line). The raw curves used in the corridor development are also shown in blue. A reasonable agreement was achieved between the FE model and experiments.

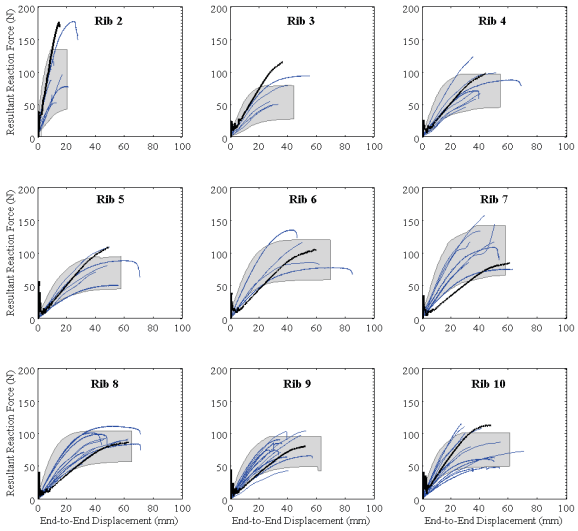

Figure 6 - Comparison of rib segment FE model (black) and experimental corridors (gray). Raw data curves are shown in blue.

Rib ring anterior-posterior loading. The sensitivity results are shown in Figure 7. It was observed that variation in the costal cartilage modulus E_{cart} produced the largest variation in reaction force, tripling the final reaction force when the modulus was increased by 100, relative to the baseline. Decreasing the modulus by 100 yielded an even more dramatic change—the final reaction force decreased by a factor of over 22, to a final value that was only 4.5% of the baseline reaction force. Changes in the joint stiffness scaling parameter λ had a modest effect on the final reaction force: $\lambda = 100$ yielded an 11.5% increase in the force, while $\lambda = 0.01$ decreased the force by only 4.5%. Changes in the sternum modulus $E_{sternum}$ resulted in changes of +32% and –6% for 100-fold increases and decreases, respectively, in the elastic modulus. As a result, it was concluded that the elastic modulus of the cartilage would be fixed at 50 MPa (to stay within the realistic range reported by Forman (2009)) to achieve the desired force-deformation response. It was also found, contrary to what was originally expected when this validation process was begun, that the stiffness of the costovertebral joints cannot be effectively validated under this loading condition—at least not at the relatively low levels of sternal deformation performed in the experiment. Instead, the cartilage modulus is the material parameter best validated using this experimental data. In addition, by comparing FE model prediction to the experiments, two general trends were observed in the rib ring model results (Figure 8): first, for rib levels 2-5, the FE model consistently indicated a more compliant response than the experimental subjects. This was more pronounced in the anterior-posterior and resultant forces than in the superior forces. Second, rib ring 1 was markedly stiffer than the experimental subjects.

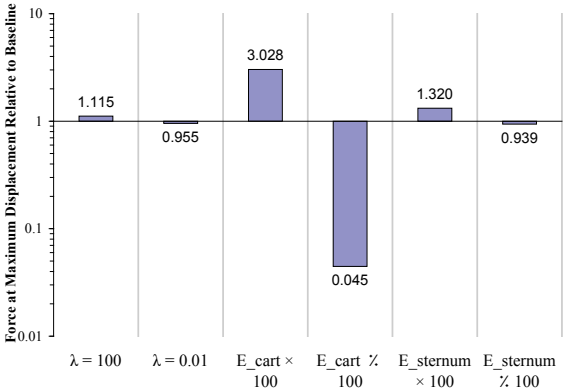

Figure 7 - Sensitivity of resultant reaction force to various material property changes, relative to the baseline force. Note that the ordinate axis is logarithmically scaled.

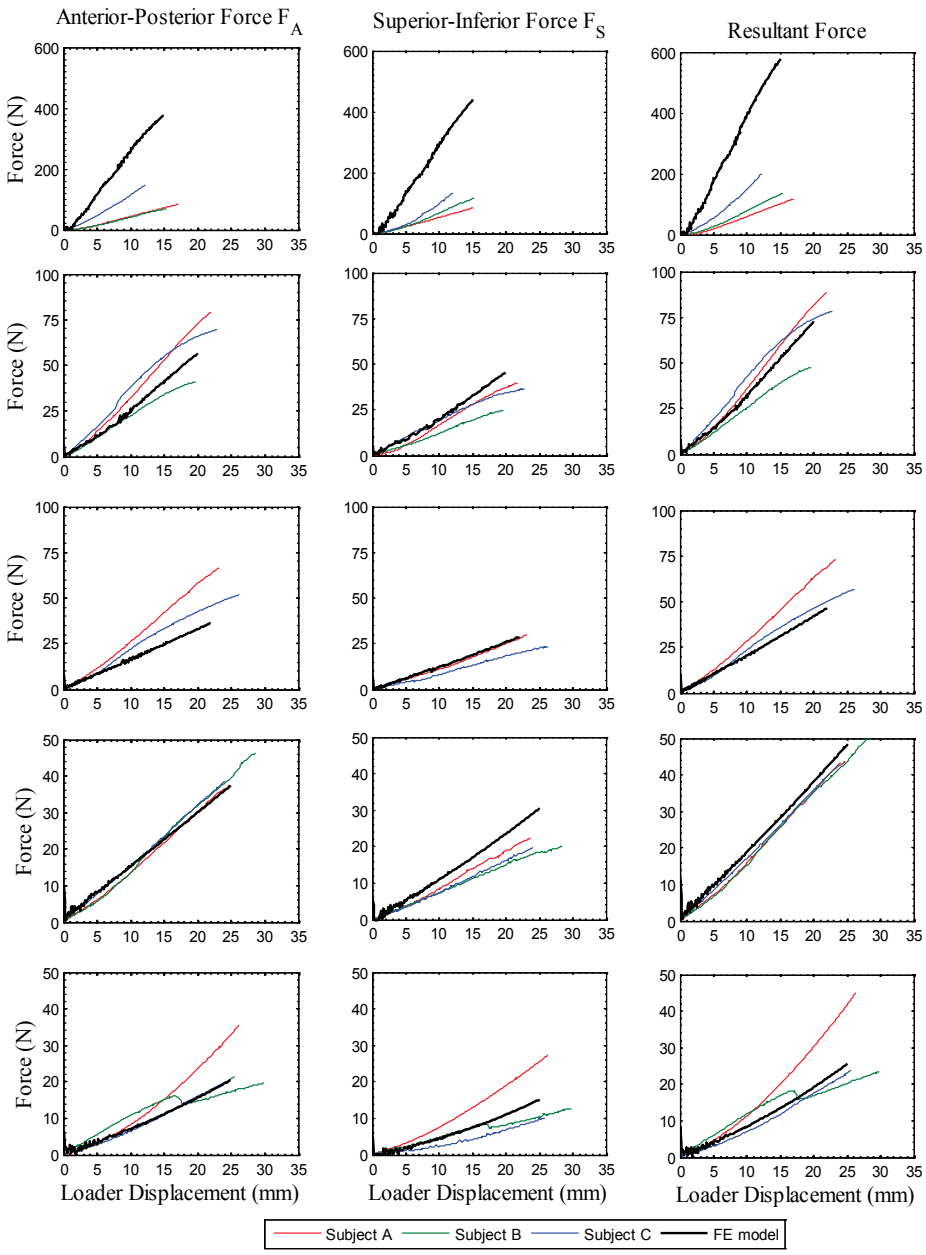

Figure 8 - Force-displacement curves of FE model compared to experimental data, using a cartilage elastic modulus of 50 MPa.

DISCUSSION

The hierarchical approach proposed in the development of the thorax model allows for evaluating the response of each individual components based on available experimental data before assessing the biomechanical response of the whole 'assembly'. In particular, the approach allows for separating the actual mechanical model from the numerical model: interactions and contacts have to be defined between components once the ribcage and the soft tissues (muscles, heart, lungs, etc…) will be included. In addition, the structural (extrinsic) response of the ribcage can be assessed independently from the response of the individual components (intrinsic response).

The third stage in validation (not completed at this time) is the point loading tests onto the eviscerated ribcage. It is briefly described here. In these experiments, the ribcage was isolated from the rest

of the thorax and tested. A full description of the method and data for this test was provided in Kindig *et al.* (2010). Three post-mortem human subjects were prepared by removing the head, extremities, superficial musculature, and visceral contents, such that only the ribcage, vertebral column, and pelvis remained. The vertebral bodies were rigidly secured to a support structure that was maintained fixed during the experiment. The loading procedure was designed to load the ribcage with a point force (Figure 9, left). This was accomplished through a novel method designed to impose few constraints upon the motion of the rib under the anterior loading. Specifically, it was intended that a purely normal force would be applied to the surface of the rib, without introducing a torque or shear force onto the rib. To this end, segments of spherical Delrin® (polyoxymethylene) glued to the rib cage at the location of loading were used as an interface between the vertical aluminum loading plate and the superficial surface of the ribcage. Translation of the plate towards the ribcage thereby, produced rotation and translation of the spherical segment. Sternal displacement was applied at 2 mm/sec to a maximum displacement of 15% of the depth at the loaded rib level. The FE model of the ribcage was developed by replicating the fixed spine boundary condition with same loading rate of 2 mm/s as the experiments in upper sternum loading at rib level 2 (Figure 9, right). The resultant contact force-displacement curve between the loading plate and the sphere will be compared to the measured experimental curve for model validation.

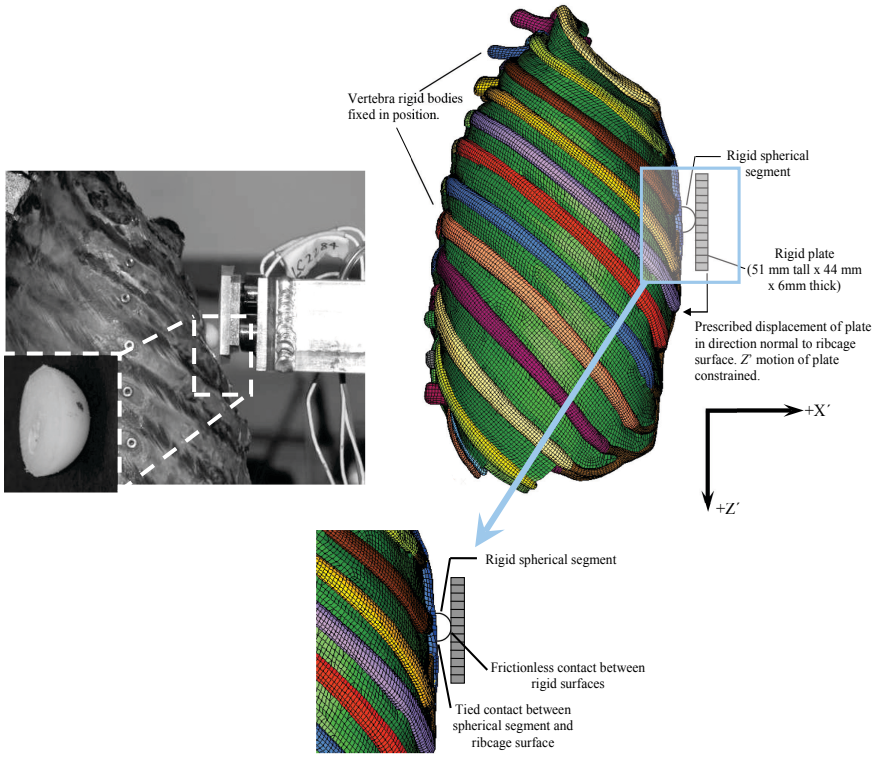

Figure 9 - Experimental setup for ribcage point loading (left) and ribcage FE model (right).

CONCLUSIONS

This study reports the ongoing development and validation progress of the GHBMC thorax model. Multi-block purely hex mesh was used for mesh generation to obtain high and consistent element quality. The rib cage model development focused on the cortical shell thickness continuously variable lengthwise and edgewise length of the ribs. The modeling method that includes high quality hexahedral element meshing, cortical thickness mapping and a hierarchical structural level validation would be helpful for the development of subject-specific thorax models. The these models are expected to provide a better understanding of the biomechanics and injury mechanisms of the thoracic structures in real crash environments and other traumatic loadings. Stability assessments and further benchmarking are underway for the GHBMC thorax model, to include impact and dynamic loading to injurious levels.

ACKNOWLEDGEMENTS

Financial support for the modeling portion in this study was provided by the Global Human Body Models Consortium, LLC (UVA: TM-001).

REFERENCES

ARNOUX, P.J., KANG, H.S., and KAYVANTASH, K. (2001). The Radioss model for Safety. Archives of Physiology and Biochemistry, 109-109.

BAUDRIT, P, HAMON, J., SONG, E, ROBIN, S., and Le COZ, J.Y. (1999). Comparative studies of dummies and human body models in frontal and lateral impact conditions. Proceedings of 43rd Stapp Car Crash Conference, Paper 99SC05.

BROSSON, B., 1989. Age and injury severity. Scand J Soc Med 1989;17(4), 287-290.

BULGER, E.M., ARNESON, M.A., MOCK, C.N., JURKOVICH, G.J., 2000. Rib Fractures in the Elderly. The Journal of Trauma: Injury, Infection, and Critical Care 48 (6),1040-1047.

CAMPBELL, B., CRONIN, D., DENG,Y.C., 2009. Coupled human body side impact model to predict thoracic injury. Proceeding of the 21th Enhanced Safety of Vehicle Conference, paper 09-0255.

CAVANAUGH, J.M., 1993. The biomechanics of thoracic trauma. In: Accidental Injury Biomechanics and Prevention, ed A.M., Nahum and J.W., Melvin, 362-390. Springer-Verlag, New York.

CHARPAIL, E., TROSSEILE, X., PETIT, P., LAPORTE, S., LAVASTE, F., 2005. Characterization of PMHS ribs: a new test methodology. Stapp Car Crash Journal 49, 183-198.

CHOI, Y.C., and Lee, I. (2009). Thorax FE model for older population. Japanese Society of Mechanical Engineers (JSME), Fukuoka

DUPREY, S., SUBIT, D., GUILLEMOT, H., KENT, R.W., (2010). Biomechanical properties of the costovertebral joint. Medical Engineering and Physics 32, 222-227.

E1-JAWAHRI, R.E., LAITURI, T.R., RUAN, J.S., ROUHANA, S.W., AND BARBAT, S.D., 2010. Development of age-dependent FE human models of a mid-sized male thorax. Stapp Car Crash Journal 54, 407-430.

FORBES, P.A., CRONIN, D.S., DENG, Y-C, 2006. Multi-Scale Human Body Model to Predict Side Impact Thoracic Trauma, International Journal of Crashworthiness,11(3) 2006, pp 203-216.

FORMAN, J.L., DEL POZO DE DIOS, E., KENT, R.W. (2010). A Pseudo-Elastic Effective Material Property Representation of the Costal Cartilage for Use in Finite Element Models of the Whole Human Body. Traffic Injury Prevention 11(6), 613 - 622

GAYZIK, F., et al., Multi‐Modality Image Data Collection Protocol for Full Body Finite Element Model Development, in SAE Digital Human Modeling. 2009, SAE: Gothenburg, Sweden.

GROSLAND, N.M., SHIVANNA, K.H., and MAGNOTTA, V.A. (2009). IA-FEMesh: an open source, interactive, multi-block approach to anatomic finite element model development. Computer Methods and Programs in Biomedicine 94, 96-107.

ITO, O., DOKKO,Y., and OHASHI, K. (2009). Development of adult and elderly FE thorax skeletal models, SAE International 2009-01-0381.

IWAMOTO, M., KISANUKI, Y., WATANABE, I., FURUSU, K., MIKI, K., AND HASEGAWA, J. (2002). Development of a finite element model of the total human body model for safety (THUMS) and application to injury reconstruction. Proceedings of Impact Research Council on the Biomechanics of Impact (IRCOBI), Munich, Germany, pp. 31-42.

KENT, R., LEE, S., DARVUSH, K., WANG, S., POSTER, C., LANGE, A., BREDE, C., LANGE, D., and MATSUOKA, F. (2005). Structural and material changes in the aging thorax and their role in crash protection for older occupants. Stapp Car Crash Journal, 49, 231-249.

KENT, R., (2008). Frontal thoracic response to dynamic loading: the role of superficial tissues, viscera and the rib cage. International Journal of Crashworthiness 13(3), 289-300. (Three tissue states investigated: intact, denuded and eviscerated)

KIMPARA, H., LEE, J.B., YANG, K.H., and KING, A.I. (2005). Development of a three-dimensional finite element chest model for the 5th percentile female. Stapp Car Crash Journal 49, 251-269.

KINDIG, M.W., Kent, R.W., (2010). Structural Response of Cadaveric Ribcages under a Localized Loading: Stiffness and Kinematic Trends. Stapp Car Crash Journal 54.

LI, Z., KINDIG, M., KERRIGAN, J.W., UNTARIOU, C.D., SUBIT D., CRANDALL, J.R., KENT, R.W., 2010. Rib fractures under anterior-posterior dynamic loads: experimental and finite element study. Journal of Biomechanics 2010; 43(2):228-234.

Li, Z., KINDIG, M.W., SUBIT, D., and KENT, R.W. (2010). Influence of mesh density, cortical thickness and material properties on human rib fracture prediction. Medical Engineering & Physics in review 32(9), 998-1008.

LIZEE, E., ROBIN, S., SONG, E., BERTHOLON, N., LECOZ, J.Y., BESNAULT, B., LAVASTE, F., 1998. Development of a 3D finite element model of the human body. Proc. 42nd Stapp Car Crash Conference, pp. 115-138. Society of Automotive Engineers, Warrendale, PA.

MOHR, M., ABRAMS, E., ENNGEL, C., LONG, W.B., and BOTTLANG, M. (2007). Geometry of human ribs pertinent to orthopedic chest-wall reconstruction. Journal of Biomechanics 40, 1310-1317.

MORRIS, A., WELSH, R., FRAMPTON, R., CHARLYON, J. and FILDES, B., 2002. An overview of requirements for the crash protection of older drivers. Proceedings of the Association for the Advancement of Automotive Medicine 46, 141-156.

PANJABI, M.M., BRAND, R.A., and WHITE, A.A., 1976. Mechanical properties of the human thoracic spine. J. Bone Joint Surg. AM, 58, p 642-652,

PATTIMORE, D., THOMAS, P., and DAVE, S. (1992). Torso Injury patterns and mechanisms in car crashes: an additional diagnostic tool. Injury: the British Journal of Accident Surgery 23(2), 123-126.

PLANK, G. R., AND EPPINGER, R. (1991). An improved finite element model of the human thorax. The 13th Proceedings of International Technical Conference on Experimental Safety Vehicles, 902-907, Paper Number S8-O-09.

RIDELLA, R.A., KUPPA, S.M., MARTIN, P.G., MCCULLOUGH, C.A., RUDD, R.W., SCABORO, M. and TAKHOUNTS, E.G. (2007). NHTSA's vision for human injury research. In: Proceedings of the 20th internationall Technical Conference on the Enhanced Safety of Vehicles. Paper number 07-0043, Lyon, France, June, 2007.

ROBIN, S. (2001). HUMOS: Human Model for Safety-A joint effort towards the development of refined human-like car occupant models. Proceedings of 17th International Technical Conference on the Enhanced Safety Vehicle, Paper 297.

RUAN, J. El-JAWAHRI, R., CHAI, L., BARBAT, S., and PRASAD, P. (2003). Prediction and analysis of human thoracic impact responses and injuries in cadaver impacts using a full human body finite element model. Stapp Car Crash Journal 47, 299-321.

SHAH, C.S., YANG, K., HARDY, W., WANG, H.K., and KING, A.I., 2001. Development of a computer model to predict aortic rupture due to impact loading. Stapp Car Crash Journal, 45, 161-182.

SONG E, TROSSEILLE, X, and BAUDRIT, P. (2009). Evaluation of thoracic deflection as injury criterion for side impact using a finite elements Thorax model. Stapp Car Crash Journal 53:155-191.

STAWICKI, S.P., GROSSMAN M.D., HOEY, B.A, MILLER D.L., AND REED, J.F. (2004). Rib fractures in the elderly: a marker of injury severity. J Am Geriatr Soc. 52(5), 805-808.

STITZEL, J.D., KILGO, P.D, WEAVER, A.A., MARTIN, R.S., LOFTIS, K.L., and MEREDITH, J.W. (2010). Age thresholds for increased mortality of predominant crash induced thoracic injuries. Ann Adv Automot Med., 54, 41-50.

TAUMURA, K., WATANABLE, I., and MIKI, K., (2005). Ederly human thoracic FE development and validation. Proceedings of 18th ESV technical conference, Paper number 05-0229.

VEZIN, P., AND BERTHET, F., (2009). Structural characterization of human rib cage behavior under dynamic loading. Stapp Car Crash Journal 53, 93-125.

WANG, S., (2000). Emerging patterns of thoracic injuries in motor vehicle crashes, 2000. Quarterly CIREN Meeting. National Highway Traffic Safety Administration (NHTSA), Washington, DC.

ZHAO, J., and NARWANI, G. (2005). Development of a human body finite element model for restraint system R&D applications. In: Proceedings of the 19th International Technical Conference on the Enhanced Safety of Vehicles (ESV) - Washington D.C., June 6-9. Paper 05-0399, 2005.